

TRANSITION METAL IMPURITIES IN SILICON

C.A.J. Ammerlaan and T. Gregorkiewicz

Natuurkundig Laboratorium, Universiteit van Amsterdam
Valckenierstraat 65, 1018 XE Amsterdam, The Netherlands

Abstract

Magnetic resonance has made significant contributions to the characterisation of point defects and small aggregates in semiconductors. A particularly clear demonstration of the potential of this technique is provided by research on transition metals in silicon. Basic atomic and electronic structural information of these centres was revealed by magnetic resonance. Two aspects of such studies, both dealing with the degree of covalency of the 3d transition metal impurity iron in silicon, will be discussed in the present paper. The fine structure in the electron paramagnetic resonance (EPR) spectra is analysed by taking into account the crystal field of the relevant symmetry and spin-orbit interaction. Agreement with experimental data requires significant covalent delocalisation of impurity electrons. This is then directly verified and confirmed by electron nuclear double resonance (ENDOR). From the hyperfine interactions with the ligand $^{29}\text{-silicon}$ nuclei the spin density around the impurity is mapped in detail. Consistent with the observed delocalisation the central impurity hyperfine coupling is reduced considerably when compared with the free-ion value.

1. Introduction

Magnetic resonance can provide detailed information on the atomic and electronic structure of paramagnetic impurities in a diamagnetic host crystal. By applying a magnetic field energy levels are split into magnetic sublevels, an interaction known as the Zeeman effect. The splitting is quantitatively described by the spectroscopic splitting tensor, more commonly called the g-tensor. The tensor is usually measured by electron paramagnetic resonance (EPR). The structure of the tensor directly provides a classification of the symmetry of the defect in terms of a crystallographic system. The principal values of the g-tensor will deviate from the free-electron value $g_e = 2.0023$, for a spin $S = 1/2$ system, if orbital contributions to the magnetism are present. For higher values of the spin, effects of orbital momentum

manifest themselves through crystal fields based on higher-order interactions. In these cases the g-values bear information on the orbital structure of the centre. This information is, however, usually difficult to extract, as knowledge on wave functions and energy levels of ground and excited states is required [1]. The use of the g-tensor to gain a detailed insight into defect structure is therefore rare. The present paper will attempt to carry out such an analysis for the specific case of positively charged iron in silicon.

As opposed to the fine structure with its related g-tensor, the interpretation of hyperfine interactions is much more straightforward. These interactions, specified by the A-tensors, can be measured with great precision and over a wide range of coupling strengths, by the method of electron nuclear double resonance (ENDOR). From these hyperfine data the distribution of spin and charge around the impurity can be mapped in great detail [2,3,4,5]. Section 3 of this paper will present such an analysis, also for positive iron in silicon, and the consistency with the results from the g-tensor data will be checked.

Besides the information based on experimental research methods, in recent years the theoretical description of impurities in semiconductor hosts has made considerable progress. Recent calculations have employed Green's function methods to solve the Schrödinger equation [6], or the multiple scattering $X\alpha$ method in a molecular cluster model [7], all in a self-consistent manner. The detailed discussion of these results is beyond the scope of the present paper.

2. Fine structure

2.1 Axial crystal field

Iron as an impurity in silicon will occupy interstitial lattice sites. According to the Ludwig and Woodbury model all valence electrons are transferred to the 3d-shell [8]. In the positive charge state the iron ion has configuration $3d^7$. With parallel exchange coupling of the three holes in the d-shell the spin of the centre is $S=3/2$. The triplet ground state has effective orbital momentum $l'=1$. Iron in this isolated form has been observed by EPR [9,10]. Besides, EPR observations have been made for complexes where iron has formed an impurity pair with an acceptor on a substitutional lattice site [10,11,12,13]. In table I the g-tensors of these centres are given. In addition, two other centres, A27 and A28, which appear to have a related structure, are mentioned [14]. In all cases the analysis of the EPR spectra has used effective spin $J=1/2$. As table I shows an interesting set of g-

values, ranging from as low as 0.59 to as high as 6.389 is found in the experiments. Their interpretation is a challenge for the theoretical analysis.

Table I. Spectroscopic data for positive interstitial iron and related complexes in silicon.

Centre	Symmetry	g-Values			α	Δ_{ax} (meV)	Δ_{rh} (meV)
		g_z	g_x	g_y			
Fe	Cubic	3.524	3.524	3.524	-0.286	0	0
FeB	Trigonal	2.0676	4.0904	4.0904	-0.256	-16	0
FeAl(1)	Trigonal	6.389	1.138	1.138	-0.346	+43	0
	(2) Orthorhombic-I	5.885	1.236	1.612	-0.3	+66	13
	(3) Orthorhombic-I	1.73	2.51	5.36			
FeGa(1)	Trigonal	5.087	2.530	2.530	-0.284	+11	0
	(2) Orthorhombic-I	6.19	0.59	0.69			
	(3) Orthorhombic-I	2.02	3.37	4.65			
FeIn	Orthorhombic-I	2.070	3.78	4.40	-0.268	-16	1.3
A27	Monoclinic-I	1.96	3.24	4.78	-0.188	-13	2.6
A28	Monoclinic-I	2.15	4.10	4.20	-0.360	-18	0.3

Table II. Spectroscopic data for positive interstitial iron and related complexes in silicon, in axial approximation.

Centre	Symmetry	g-Values		α	x	$\Delta_{ax}/\alpha\lambda$	Δ_{ax} (meV)
		g_{\parallel}	g_{\perp}				
Fe	Cubic	3.524	3.524	-0.286	2	0	0
FeB	Trigonal	2.0676	4.0904	-0.256	7.513	-4.44	-16
FeAl(1)	Trigonal	6.389	1.138	-0.346	0.318	+8.71	+43
	(2) Orthorhombic-I	5.885	1.424	-0.165	0.420	+7.08	+17
	(3) Orthorhombic-I	1.73	3.935				
FeGa(1)	Trigonal	5.087	2.530	-0.284	0.933	+2.61	+11
	(2) Orthorhombic-I	6.19	0.64	-0.140	0.170	+17.91	+36
	(3) Orthorhombic-I	2.02	4.01				
FeIn	Orthorhombic-I	2.070	4.09	-0.256	7.444	-4.40	-16
A27	Monoclinic-I	1.96	4.01	-	-	-	-
A28	Monoclinic-I	2.15	4.15	-0.360	6.029	-3.52	-18

Although some of the centres actually have lower symmetry they will all be treated as axial in a first analysis. This assumption will allow an analytical more transparent treatment, which is presented first. Where necessary the tensors of the lower symmetry centres will be forced to appear as axial by averaging the two g -values which are already closely equal in several cases. An approximate perpendicular

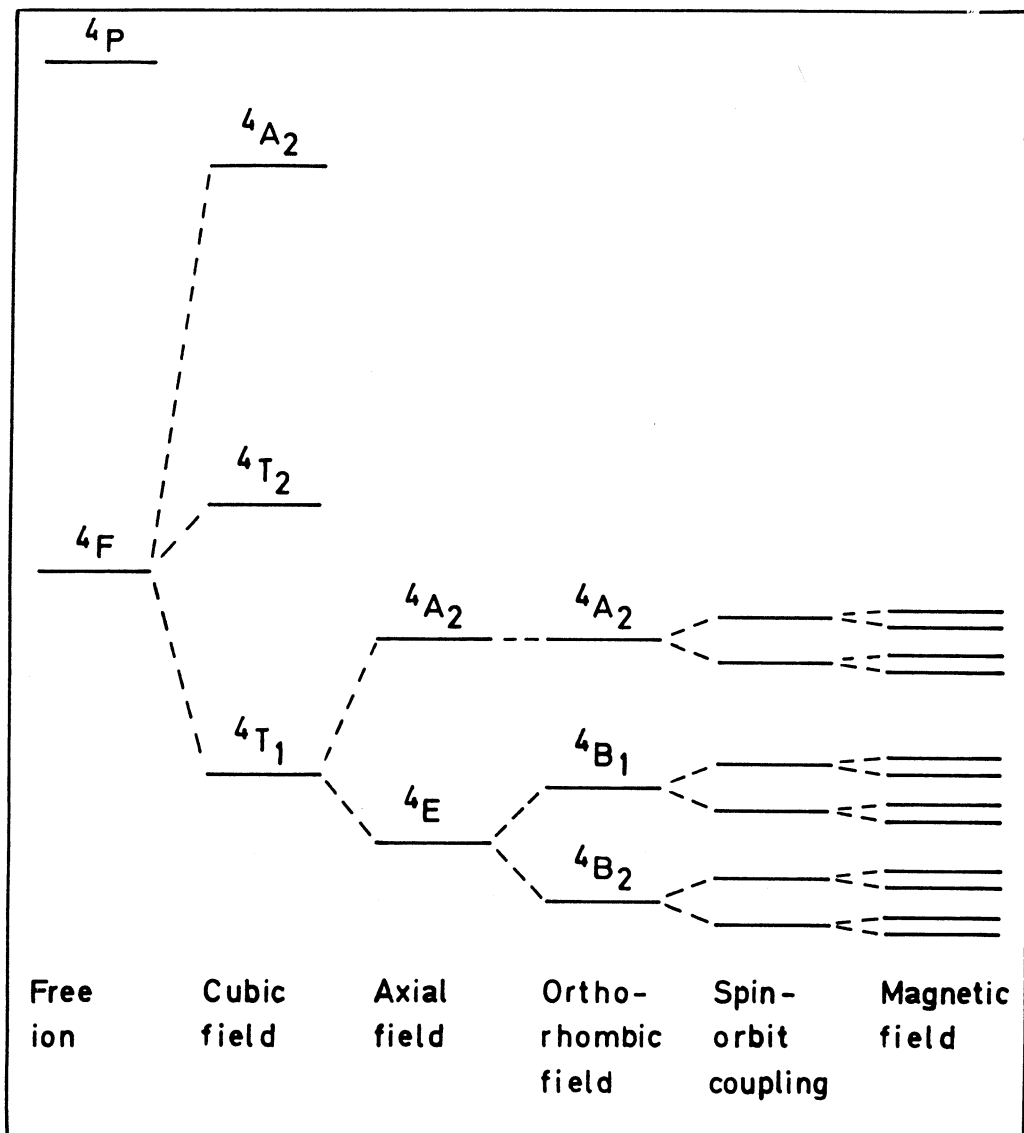


Fig. 1 Energy level diagram for the Fe^+ -ion in electronic configuration $3d$.

g-value g_{\perp} is defined as $g_{\perp} = (g_x + g_y)/2$. The resulting data are found in table II. The more general case taking account of the orthorhombic or monoclinic symmetry, which requires computer methods to be solved, will be discussed more briefly in paragraph 2.2.

Figure 1 presents a schematic energy level diagram of positive iron, electronic configuration $3d^7$, on an interstitial site in a silicon crystal. The free-ion ground state 4F is split by the cubic crystal field (cf) leaving a 12-fold degenerate 4T_1 state lowest. In complexes of lower than cubic symmetry the crystal field, of trigonal or orthorhombic symmetry, will further split this level. Spin-orbit (so) interaction will finally lift the four-fold spin degeneracy, resulting in the splitting of the 4T_1 level into six Kramers doublets. These interactions are represented by the spin-hamiltonian H:

$$H = H_{cf} + H_{so}, \quad (1)$$

$$H_{cf} = +\Delta_{ax} (2/3 - l_z^2), \quad (2)$$

$$H_{so} = +\alpha\lambda(l_x' s_x + l_y' s_y + l_z' s_z). \quad (3)$$

The hamiltonian will operate on the twelve basis states of the 4T_1 ground state in cubic symmetry. This state which is orbitally three-fold degenerate, will have an effective angular momentum $l'=1$. The associated orbital g-factor giving the magnetic moment has the theoretical value $\alpha=-3/2$. To find eigenstates and corresponding energies the 12×12 matrix $\langle {}^4T_1 | H | {}^4T_1 \rangle$ has to be diagonalised. Due to the Kramers degeneracy there are actually two identical 6×6 matrices. These are found from table III by setting Δ_{rh} equal to zero. By forming suitable linear combinations the matrix can be decomposed into one cubic, one quadratic and one linear matrix, as specified in table IV. The solution of the associated eigenvalue equations does not present any special problem. The energies E_1 to E_6 of the doublets as a function of the axial field strength Δ_{ax} , both in units $\alpha\lambda$, are presented as figure 2. For iron in $3d^7$ configuration the spin-orbit coupling constant λ is negative. Having found these solutions the effect of a magnetic field \vec{B} can now be evaluated. The hamiltonian of the Zeeman effect, treated as a small perturbation on the doublets, has the orbital and spin parts

$$H_{mf} = +\alpha\mu_B \vec{B} \cdot \vec{l}' + 2\mu_B \vec{B} \cdot \vec{s}. \quad (4)$$

Table III. Matrix elements of the crystalline field, axial and orthorhombic, and spin-orbit coupling in the 4T_1 state.

	$ -x,+3/2\rangle$	$ iy,+3/2\rangle$	$ -x,-1/2\rangle$	$ iy,-1/2\rangle$	$ +z,-3/2\rangle$	$ +z,+1/2\rangle$
	$ +x,-3/2\rangle$	$ iy,-3/2\rangle$	$ +x,+1/2\rangle$	$ iy,+1/2\rangle$	$ +z,+3/2\rangle$	$ +z,-1/2\rangle$
$\langle -x,+3/2 $ $\langle +x,-3/2 $	$-\Delta_{rh} - \Delta_{ax}/3$	$-3\alpha\lambda/2$	0	0	0	$-\sqrt{3}\alpha\lambda/2$
$\langle -iy,+3/2 $ $\langle -iy,-3/2 $	$-3\alpha\lambda/2$	$+\Delta_{rh} - \Delta_{ax}/3$	0	0	0	$-\sqrt{3}\alpha\lambda/2$
$\langle -x,-1/2 $ $\langle +x,+1/2 $	0	0	$-\Delta_{rh} - \Delta_{ax}/3$	$+\alpha\lambda/2$	$-\sqrt{3}\alpha\lambda/2$	$+\alpha\lambda$
$\langle -iy,-1/2 $ $\langle -iy,+1/2 $	0	0	$+\alpha\lambda/2$	$+\Delta_{rh} - \Delta_{ax}/3$	$-\sqrt{3}\alpha\lambda/2$	$-\alpha\lambda$
$\langle +z,-3/2 $ $\langle +z,+3/2 $	0	0	$-\sqrt{3}\alpha\lambda/2$	$-\sqrt{3}\alpha\lambda/2$	$+2\Delta_{ax}/3$	0
$\langle +z,+1/2 $ $\langle +z,-1/2 $	$-\sqrt{3}\alpha\lambda/2$	$-\sqrt{3}\alpha\lambda/2$	$+\alpha\lambda$	$-\alpha\lambda$	0	$+2\Delta_{ax}/3$

The magnetic field will lift the remaining Kramers degeneracy in the doublets as shown in figure 1. Usually, the magnetic resonance experiment is carried out between the levels originating from the ground state doublet. Figure 2 shows that irrespective of the sign or strength of the axial field the doublet E_1 always has lowest energy. For this ground state, which is derived from the cubic equation, the results for the g-tensor are summarised by

$$\Delta_{ax}/\alpha\lambda = -(x-2)(x+1)(x+6)/2x(x+2), \quad (5)$$

$$E/\alpha\lambda = -(x^3+5x^2+13x+6)/3x(x+2), \quad (6)$$

$$g_{\parallel} = +2[x^4+4x^3+14x^2+72x+72+2\alpha(x^2-12x-12)]/(x^4+4x^3+18x^2+24x+24), \quad (7)$$

$$g_{\perp} = +4[x^4+4x^3+16x^2+24x-2\alpha x^2(x+2)]/(x^4+4x^3+18x^2+24x+24). \quad (8)$$

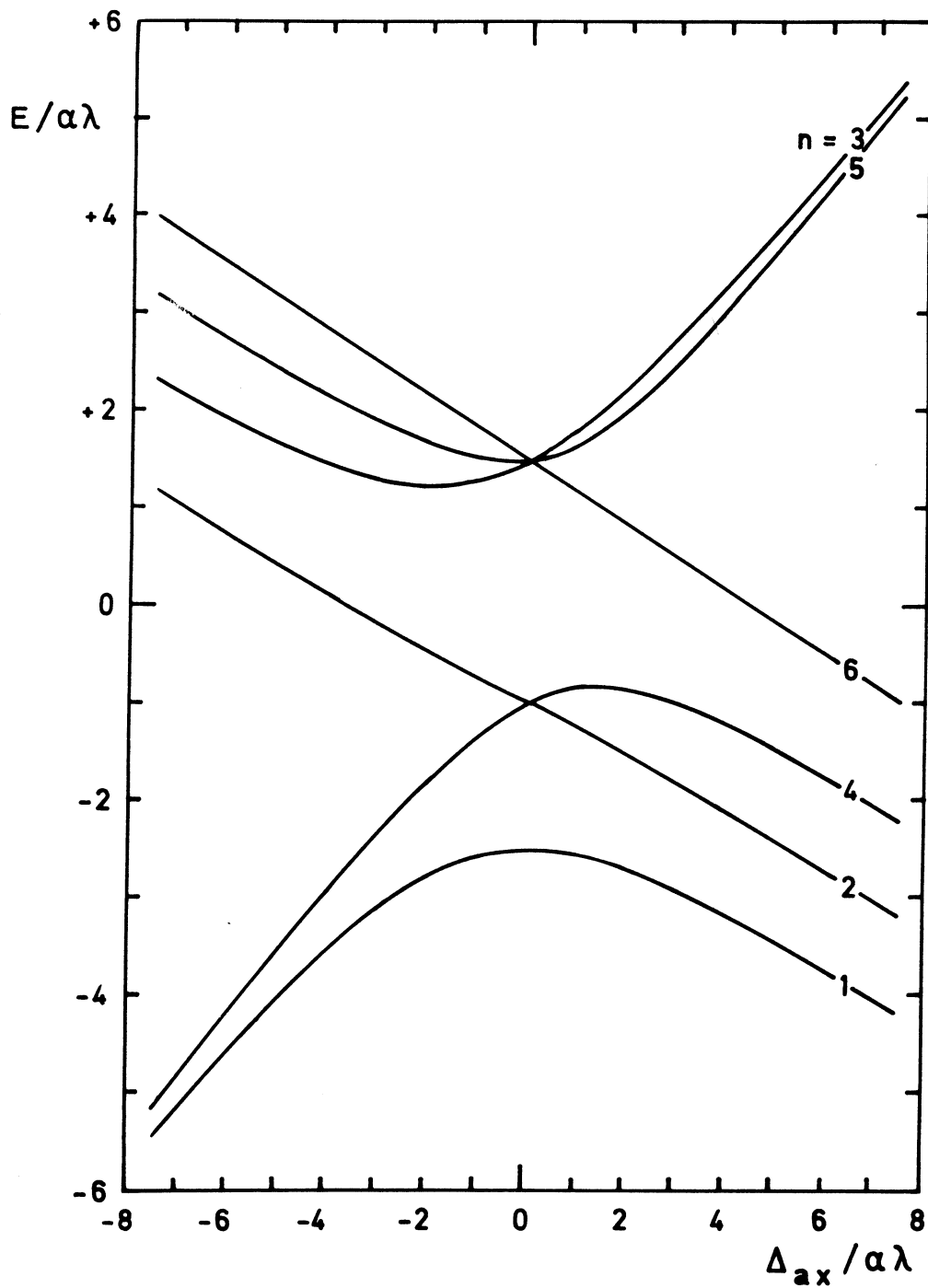


Fig. 2 Energy positions E , in units $\alpha\lambda$, of the six Kramer doublets, labelled $n=1, \dots, 6$, as a function of the trigonal crystal field, in reduced units $\Delta_{ax}/\alpha\lambda$.

Table IV. Matrix elements of the axial crystalline field and spin-orbit coupling in modified 4T_1 states.

	$ -1,+3/2\rangle$ $ +1,-3/2\rangle$	$ 0,+1/2\rangle$ $ 0,-1/2\rangle$	$ +1,-1/2\rangle$ $ -1,+1/2\rangle$
$\langle -1,+3/2 $ $\langle +1,-3/2 $	$-\Delta_{ax}/3 - 3\alpha\lambda/2$	$+ \sqrt{6}\alpha\lambda/2$	0
$\langle 0,+1/2 $ $\langle 0,-1/2 $	$+ \sqrt{6}\alpha\lambda/2$	$+2\Delta_{ax}/3$	$+ \sqrt{2}\alpha\lambda$
$\langle +1,-1/2 $ $\langle -1,+1/2 $	0	$+ \sqrt{2}\alpha\lambda$	$-\Delta_{ax}/3 - \alpha\lambda/2$
	$ 0,+3/2\rangle$ $ 0,-3/2\rangle$	$ +1,+1/2\rangle$ $ -1,-1/2\rangle$	
$\langle 0,+3/2 $ $\langle 0,-3/2 $	$+2\Delta_{ax}/3$	$+ \sqrt{6}\alpha\lambda/2$	
$\langle +1,+1/2 $ $\langle -1,-1/2 $	$+ \sqrt{6}\alpha\lambda/2$	$-\Delta_{ax}/3 + \alpha\lambda/2$	
	$ +1,+3/2\rangle$ $ -1,-3/2\rangle$		
$\langle +1,+3/2 $ $\langle -1,-3/2 $	$-\Delta_{ax}/3 + 3\alpha\lambda/2$		

The dummy variable x relates the axial field Δ_{ax} to energy and g -values. A useful way to represent the result is the elimination of x between the equations (7) and (8), obtaining a direct relation between g_{\parallel} and g_{\perp} . A graphical representation of the result is given in figure 3. The special case of cubic symmetry, with $\Delta_{ax}=0$ and $x=2$, leads to $g_{\parallel}=g_{\perp}=13/3$, and is applicable for isolated interstitial iron. In the upper left corner of the plot the solutions for $\Delta_{ax}/\alpha\lambda < 0$, when the singlet level forms the ground state, are shown. The lower right part gives the solutions corresponding to $\Delta_{ax}/\alpha\lambda > 0$ and the 4E doublet ground state. Included in the figure are also the experimental data points, as taken from table II. Although a tendency of the measured g -values to follow the theoretical relationship is apparent, not an

entirely satisfactory agreement is observed. The discrepancy may be explained by a reduction of the orbital contribution to the magnetism. Complete quenching, expressed by $\alpha=0$ in the formulas and in figure 3, leads to an underestimation of the g -values. Another curve, for $\alpha=-1$ can also be justified theoretically, as will be discussed in paragraph 2.4. A best agreement is obtained for the empirical value of the orbital g -factor $\alpha=-(0.3\pm 0.05)$.

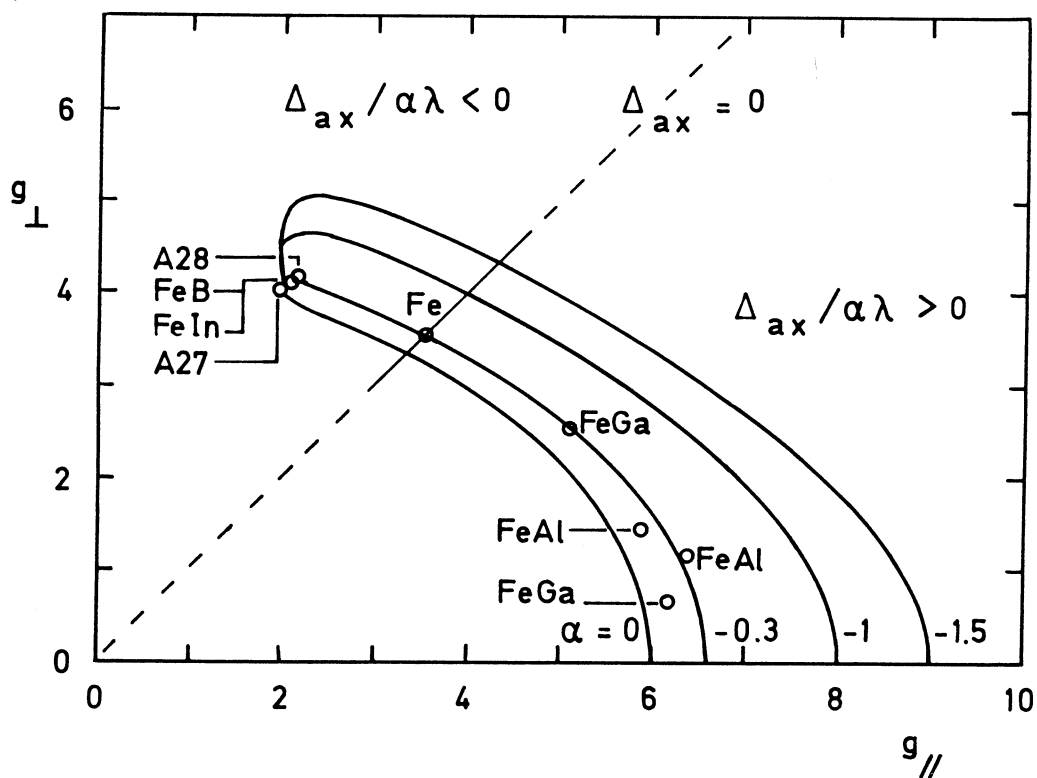


Fig. 3 Theoretical relations and experimental data for the Zeeman splitting factors g_{\parallel} and g_{\perp} for a $3d^7$ iron ion in an axial crystal field.

Some special attention may be given to the data points close to $g_{\parallel}=2$, $g_{\perp}=4$. The significance of these points may be questioned, as it is known that a spin quartet split by a strong axial field will always yield one doublet with $g_{\parallel} \approx g_e \approx 2$ and $g_{\perp} \approx 2g_e \approx 4$, in the $J=1/2$ formalism. To check more carefully on this aspect, the portion of figure 3 near $g_{\parallel}=2$ and $g_{\perp}=4$ is shown in close-up in figure 4. It shows clearly that

also the data points for these cases require a value $\alpha = -0.3$ for their interpretation.

Having selected the value $\alpha = -0.3$ an alternative way of representing the results is shown as figure 5. Again, of course, the agreement is apparent. Values for $\Delta_{ax}/\alpha\lambda$ for which this agreement is obtained can

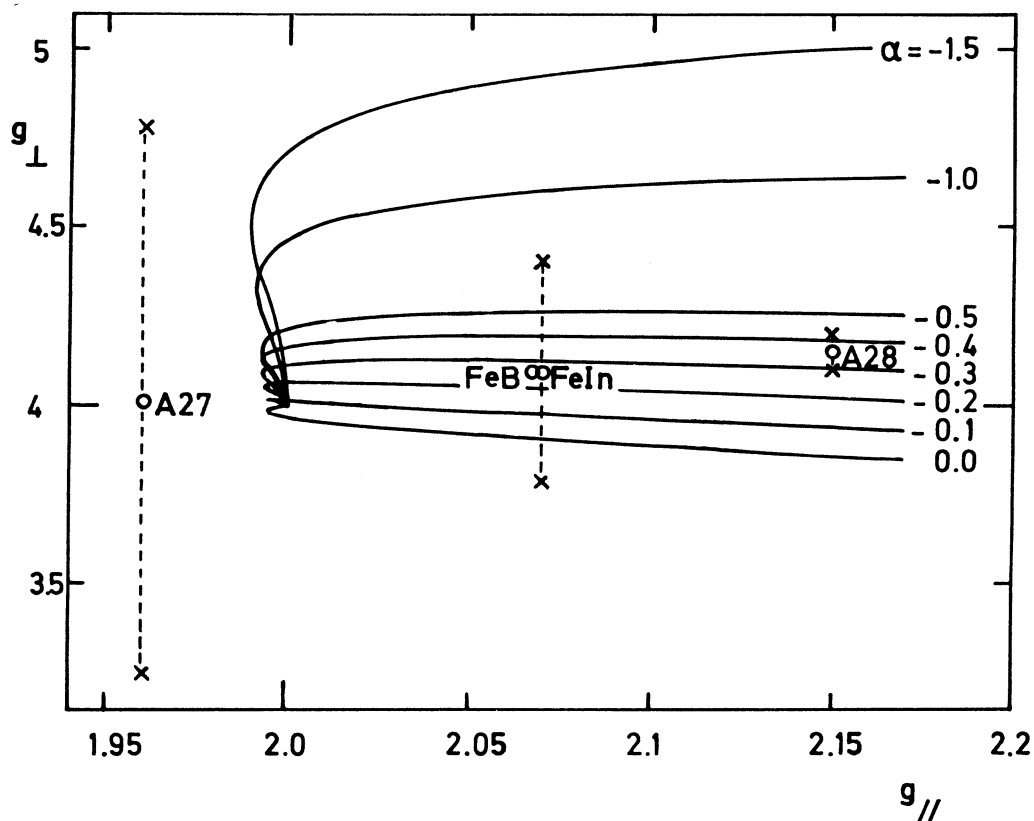


Fig. 4 Theoretical relations and experimental data for the Zeeman splitting factors g_{\perp} and g_{\parallel} for a $3d^7$ iron ion in a large axial crystal field with $\Delta_{ax}/\alpha\lambda < 0$.

be read from the bottom scale. In table II the results of the analysis are summarised. To calculate the axial field Δ_{ax} the value $\lambda = -14.3$ meV was used for the spin-orbit coupling constant [15]. In the analysis as presented the two unknown quantities α and x , or alternatively α and Δ_{ax} , are calculated from the measured quantities g_{\parallel} and g_{\perp} . If the equations allow for a solution, the agreement will then be exact.

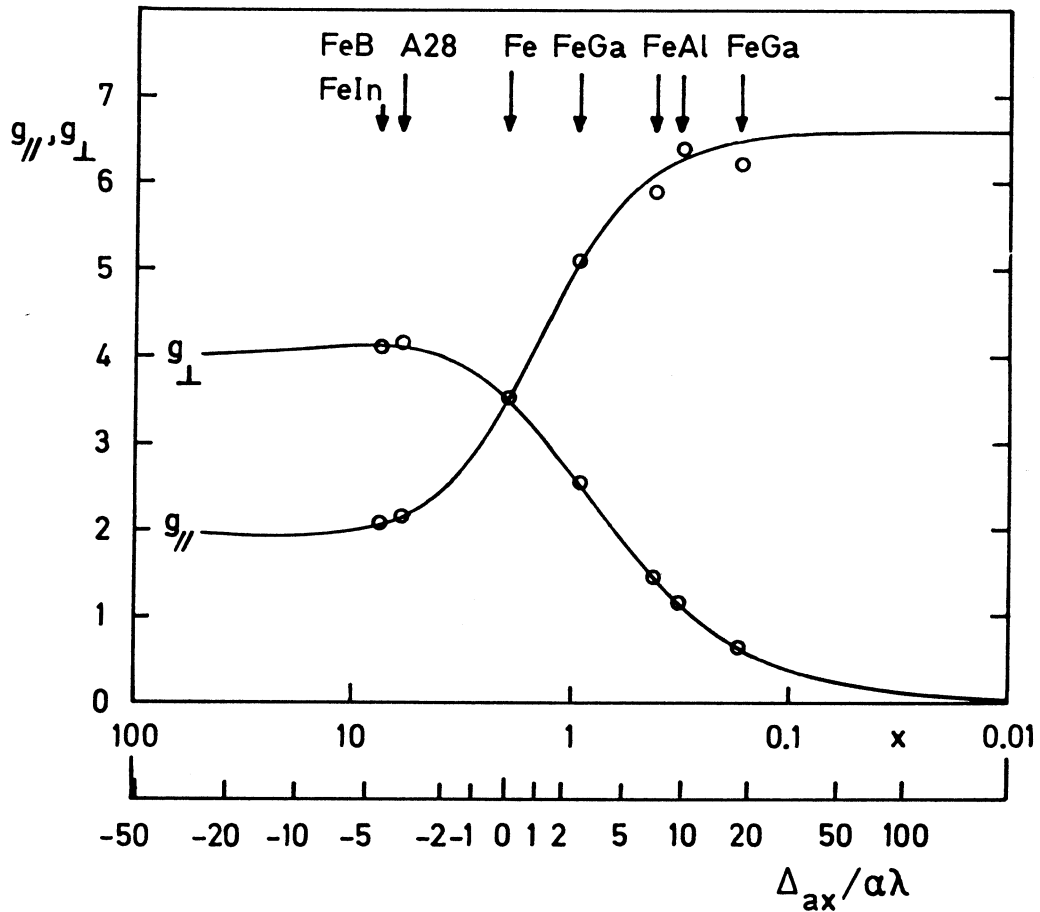


Fig. 5 Theoretical and experimental Zeeman splitting factors $g_{//}$ and g_{\perp} as a function of the axial crystal field, for an effective orbital g_{\perp} -factor $\alpha = -0.3$.

2.2 Orthorhombic crystal field

For this more general case the crystal field Hamiltonian H_{cf} takes the form

$$H_{cf} = +\Delta_{ax}(2/3 - 1_z^2) + \Delta_{rh}(1_x^2 - 1_y^2), \quad (9)$$

replacing equation (2). Operation of the orthorhombic hamiltonian on the basis states of 4T_1 will produce the matrixelements of table III. For solution of the eigenvalue equation numerical methods are required. A solution for the eigenstates can be written as

$$|+\rangle = a|-x, +3/2\rangle + b|iy, +3/2\rangle + c|-x, -1/2\rangle + d|iy, -1/2\rangle + e|+z, -3/2\rangle + f|+z, +1/2\rangle, \quad (10)$$

$$|-\rangle = a|+x, -3/2\rangle + b|iy, -3/2\rangle + c|+x, +1/2\rangle + d|iy, +1/2\rangle + e|+z, +3/2\rangle + f|+z, -1/2\rangle. \quad (11)$$

In terms of the coefficients a to f the principal g-values are derived as:

$$g_x = 2 \langle + | (+\alpha l'_x + 2S_x) | - \rangle = |-4c^2 + 4d^2 + 4f^2 - 4\sqrt{3}ac + 4\sqrt{3}bd + 4\sqrt{3}ef - \alpha(4be + 4df)|, \quad (12)$$

$$g_y = 2 \langle + | (+\alpha l'_y + 2S_y) | - \rangle = |4c^2 - 4d^2 + 4f^2 - 4\sqrt{3}ac + 4\sqrt{3}bd - 4\sqrt{3}ef + \alpha(4ae + 4cf)|, \quad (13)$$

$$g_z = 2 \langle + | (+\alpha l'_z + 2S_z) | + \rangle = |6a^2 + 6b^2 - 2c^2 - 2d^2 - 6e^2 + 2f^2 - \alpha(4ab + 4cd)|. \quad (14)$$

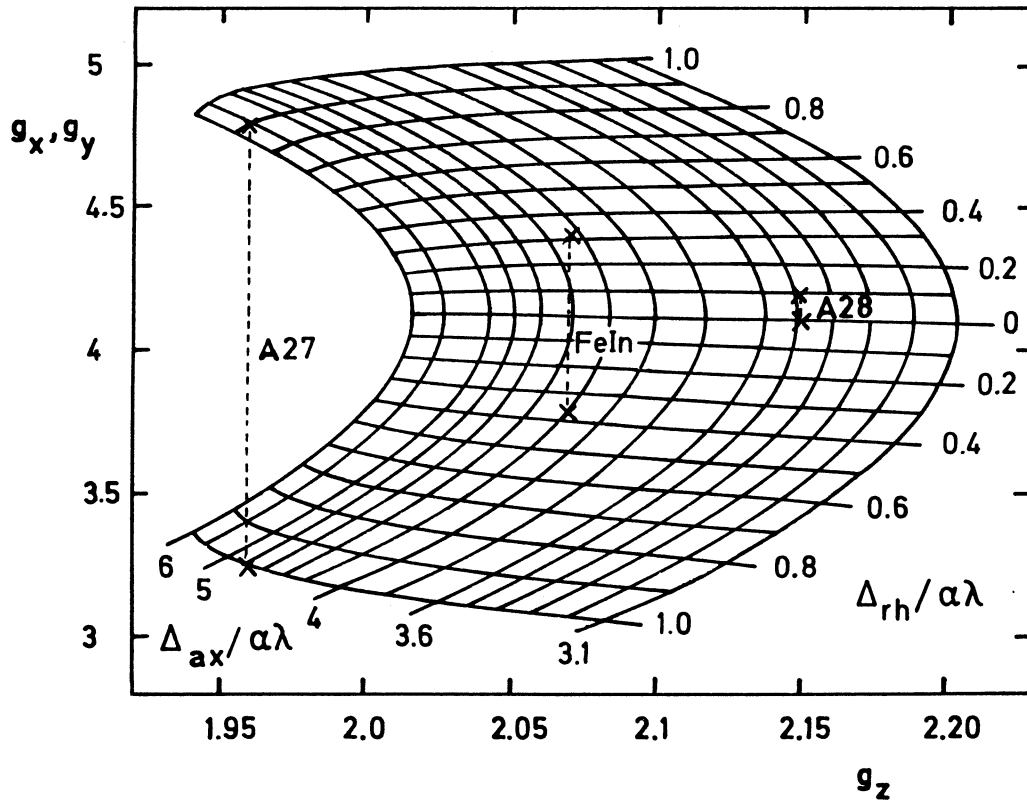


Fig. 6 Theoretical relations and experimental data for the Zeeman splitting factors near $(g_x, g_y, g_z) = (4, 4, 2)$, as a function of axial and orthorhombic crystal fields, for effective orbital g-factor $\alpha = -0.3$.

Again the number of unknowns to be determined, i.e. Δ_{ax} , Δ_{rh} and α equals the number of equations to be satisfied, i.e. for g_x , g_y and g_z . In the region near $(g_x, g_y, g_z) = (4, 4, 2)$ the solution is numerically stable. This can be illustrated by reference to the figures 4 and 6. From figure 6 it is concluded that Δ_{rh} is mainly determined by the difference $g_y - g_x$, rather independent of g_z . The average value of g_x and g_y essentially determines the factor α . The effects of α , Δ_{ax} , and Δ_{rh} are sufficiently orthogonal to allow the accurate determination of the parameters from the g-values. As a result the unambiguous solutions as given in table I are obtained for the centres A27, A28 and FeIn. The former centre for which it was not possible to find a solution in the axial approximation does not present any difficulty using the generalised crystal field of equation (9). The analysis of these orthorhombic and monoclinic centres confirms the reduced g-factor $\alpha = -0.3$. Unfortunately, in other regions of the parameter space the magnitude of α is strongly correlated with the crystal fields, and unambiguous solutions can not be obtained. For instance, the parameters $\alpha = -0.3$, $\Delta_{ax} = +66$ meV and $\Delta_{rh} = +13$ meV result in $g_x = 1.240$, $g_y = 1.609$ and $g_z = 5.885$. On the other hand, the quite different parameter selection $\alpha = -1.5$, $\Delta_{ax} = 1579$ meV and $\Delta_{rh} = 390$ meV gives $g_x = 1.238$, $g_y = 1.611$ and $g_z = 5.885$, representing a fit with comparable good agreement for the FeAl(2) spectrum. In these cases therefore the argument is reversed by requiring $\alpha = -0.3$ for consistency with other results. The crystal field parameters can then be determined.

2.3 Excited states

In figure 2 the energy levels are shown in their dependence on axial field and spin-orbit interaction. For positive values of the reduced axial field $\Delta_{ax}/\alpha\lambda$ the four doublets derived from the 4E state are lowest in energy. For large values of the crystal field the levels approach equal separation by the amount $\alpha\lambda$. With the results of the previous analysis, $\alpha = -0.3$ and $\lambda = -14.3$ meV, this can be estimated as 4.3 meV, or $T = 50K$ in temperature units. Except at the lowest temperatures, the excited levels E_2 , E_4 and E_6 may become appreciably populated thermally and resonance in them may be observable. For negative axial field the excited level E_4 even tends to coincide with the ground level E_1 . Under such conditions the observation of resonances in both doublets derived from the 4A_1 spin quartet may be expected. Also, the assumption of small Zeeman energies compared to the doublet separation may then break down. This is more quantitatively discussed by Gehlhoff, et al. [13]. These authors actually report resonances in

excited doublets for FeAl, FeGa and possibly FeIn.

2.4 Orbital g-factor

Obviously, the selection on empirical grounds of a strongly reduced effective orbital g-factor $\alpha = -0.3$ needs justification. The theoretical value $\alpha = -3/2$ reflects the transformation properties of a pure 4T_1 ground state in cubic symmetry. Any deviation from this description may lead to changes in α . In a first attempt the quenching of orbital momentum due to Jahn-Teller distortion may be considered. For isolated interstitial iron, which has cubic symmetry, with $\Delta_{ax} = 0$ and $x=2$ in equation (5), the theoretical g-value $g = (10/3) - (2/3)\alpha$ ranges from $g = 13/3$ for $\alpha = -3/2$ without any quenching, to $\alpha = 0$ and $g = 10/3$ for complete quenching of the orbital moment. The experimental value $g = 3.524$ thus corresponds to $\alpha = -0.286$ or 81% quenching. This reduction observed for iron in undistorted cubic symmetry was explained by Ham in a classical paper as a manifestation of a dynamical Jahn-Teller effect of the 4T_1 orbital triplet state [16]. Applying this concept to the pairs FeGa and FeAl one notes that also for these centres the successful analysis requires $\alpha = -0.3$. It is considered remarkable that these pairs with an E doublet ground state experience an equal Ham reduction factor as the triplet state for iron. Even more surprisingly, the pairs FeB, FeIn, and the A27 and A28 defects also have $\alpha = -0.3$. Since these centres have an A_2 orbital singlet ground state no Jahn-Teller instability and associated quenching is expected. On the basis of these results the Jahn-Teller mechanism as an explanation for the reduction of α appears unlikely. A recent theoretical analysis confirms this conclusion [17].

Modification of the ground state wave function by hybridisation offers another explanation for the reduction of α . Besides lifting the degeneracy of the 4F free-ion ground state, the cubic field also has matrixelements between the 4F and 4P terms. Some p-character, derived from the 4P term, will be admixed to the 4T_1 ground state [18]. An improved expression for the wave function is thus of the form

$$\psi = \eta_F \phi_F + \eta_P \phi_P, \quad (15)$$

normalised by $\eta_F^2 + \eta_P^2 = 1$. The effective orbital g-factor associated with the hybridised wave function is

$$\alpha = -(3/2) \eta_F^2 + \eta_P^2. \quad (16)$$

Admixture of p-functions through the cubic field has a maximum $\eta_P^2 = 0.2$.

Corresponding to this maximum, equation (16) gives a lower limit of -1 for α . Therefore, the effect of hybridisation, leading to $-3/2 \leq \alpha \leq -1$, may account for a reduction of α , but its possible effect is too small to fully explain the observed reduction to -0.3 . In addition, the lower limit $\alpha = -1$ corresponds to an infinite cubic field. A more realistic estimate for the cubic field may give it a strength comparable to the $^4P-^4F$ splitting, which equals ≈ 1.4 eV [19]. This estimate raises the lower limit of α to ≈ -1.4 .

Along similar lines the effect on the ground state wave function by covalent hybridisation with host atoms may be examined. Although the defect electrons will certainly be found in the impurity space, appreciable covalent delocalisation may occur. A recent experiment in which the electron distribution around the positive iron ion in silicon was measured by electron nuclear double resonance will be discussed in section 3 of this paper [20]. A suitable wave function may be constructed as a linear combination of 3d iron and ligand silicon orbitals:

$$\psi = \eta_{\text{Fe}} \psi_{\text{Fe}} + \eta_{\text{Si}} \psi_{\text{Si}}, \quad (17)$$

again normalised by $\eta_{\text{Fe}}^2 + \eta_{\text{Si}}^2 = 1$. In the impurity space the electrons will be described mainly by d-electrons with $\alpha = -3/2$ and, for iron, a spin-orbit coupling constant $\lambda = -14.3$ meV [15]. In the crystal around the impurity the 3p orbitals on the silicon atoms appearing in the expansion (17) will have $\alpha = +1$ and $\lambda = -20$ meV [21]. The effective orbital g-factor may be approximated by the weighted average

$$\alpha = -(3/2) \eta_{\text{Fe}}^2 + \eta_{\text{Si}}^2. \quad (18)$$

Agreement with the measured value $\alpha = -0.3$ is obtained for $\eta_{\text{Si}}^2 = 0.48$. This numerical example shows that the reduced orbital contribution can be understood by assuming considerable covalent delocalisation.

3. Hyperfine structure

3.1 LCAO analysis

To analyse the hyperfine interactions the one-electron wave function for the unpaired electrons is expanded in atomic orbitals, as indicated schematically in equation (17). At the central site the 3d orbitals of the iron impurity are included. The term $\eta_{\text{Si}} \psi_{\text{Si}}$ actually is a summation over hybrid 3s3p orbitals centered on silicon sites surrounding the impurity. For the analysis it is appropriate to decompose

the measured hyperfine interaction tensor \vec{A} into an isotropic part $a \cdot \vec{1}$, with $a = (1/3)\text{Tr}(\vec{A})$, and the remaining anisotropic tensor \vec{B} . The isotropic interaction a with a particular nucleus can then be related to contact spin density $|\phi(r)|^2$ on the site r of that nucleus. This is expressed by:

$$a = (2/3) \mu_0 g_e g_N \mu_B \mu_N |\phi(r)|^2. \quad (19)$$

Anisotropic tensor \vec{B} results from dipole-dipole interaction between the nucleus and electronic spin in the silicon 3p orbitals. The principal values of this axial tensor (2b, -b, -b) are related to the 3p-orbitals by

$$b = (2/5) (\mu_0 / 4\pi) g_e g_N \mu_B \mu_N \langle r^{-3} \rangle_{3p}. \quad (20)$$

Relations (19) and (20) allow the calculation of $|\phi(r)|^2$ and $\langle r^{-3} \rangle_{3p}$ valid for the defect electron wave function from the measured a and b . By comparison with tabulated atomic values for fully occupied orbitals [22] the coefficients in the expansion are obtained.

3.2 Impurity ENDOR

With the iron ion, i.e. with the 57-iron isotope which has nuclear spin $I=1/2$, the observed hyperfine interaction is isotropic. Its strength $a = 2.985 \times 10^{-4} \text{ cm}^{-1}$ has been measured accurately by ENDOR [23]. With equation (19) one finds $|\phi(0)|^2 = 0.25 \times 10^{30} \text{ m}^{-3}$, which is very small in comparison to the free-ion value $|\phi(0)|^2 = 5.65 \times 10^{30} \text{ m}^{-3}$. It leads to the conclusion that only about 5% of the electrons is accommodated in impurity orbitals. This result should, however, be considered with some reserve. The impurity d-orbitals themselves do not have any contact density. Their effect is only indirect through spin polarisation of the s-electrons in the core. Calculations of this process were performed by Watson and Freeman [24]. The accuracy of such calculations is not well known.

3.3 Ligand ENDOR

In a recent experiment the hyperfine interactions with ^{29}Si nuclei near the iron impurity were accurately measured by ENDOR [20]. The interactions with 98 atoms in 8 shells of symmetry related sites around the centre were resolved. Analysing these data in a one-electron model, using the equations (19) and (20), the coefficients of the expansion in silicon 3s and 3p orbitals are obtained. The total

amount of spin density transferred to the surrounding crystal space is found to be 26%, indicating substantial covalency. More than 90% of this spin density is in silicon 3p orbitals. However, adding spin densities on impurity and silicon sites, one concludes that only just over 30% of the electrons have been revealed in the ENDOR experiment. This can be understood as ENDOR measures spin density whereas charge density is required. Spin, being a vector quantity, may cancel for different electrons, while charge directly adds. A measurement of spin density may therefore severely underestimate charge density. The figure of 26% reported above represents a lower limit.

4. Conclusion

An analysis of the fine structure, measured by electron spin resonance, and of the hyperfine structure, obtained from electron nuclear double resonance, for the positively charged interstitial iron impurity in silicon was presented. The g-values describing the Zeeman splitting of the impurity, either in isolated form or as part of a complex, could be understood by considering the action of crystal field and spin-orbit coupling on the 4T_1 ground state of a $3d^7$ configuration. The reduction of the orbital g-value is most likely not related to Jahn-Teller distortions, nor to intra-atomic hybridisation on the impurity. Covalent delocalisation of the defect electrons over silicon atoms in the vicinity of the impurity may have the predominant effect. The picture of substantial covalent character is supported by the low spin density found by ENDOR on the iron ion. In addition, the extended distribution of electrons over lattice atoms is evidenced by observations in ENDOR of hyperfine interactions with 98 silicon atoms. The accurate mapping of spatial extent of the wave function is unfortunately severely hampered by differences between the spin and charge distribution, which are apparent for this many-electron system.

References

1. M.H.L. Pryce, Proc. Phys. Soc. A **63**, 25 (1950)
2. D.A. van Wezep, R. van Kemp, E.G. Sieverts and C.A.J. Ammerlaan, Phys. Rev. B **32**, 7129 (1985)
3. D.A. van Wezep, T. Gregorkiewicz, E.G. Sieverts and C.A.J. Ammerlaan, Phys. Rev. B **34**, 4511 (1986)
4. R. van Kemp, E.G. Sieverts and C.A.J. Ammerlaan, Phys. Rev. B **36**, 3528 (1987)
5. E.G. Sieverts, D.A. van Wezep, R. van Kemp and C.A.J. Ammerlaan, Mat. Science Forum 10-12, 729 (1986)

6. H. Katayama-Yoshida and A. Zunger, *Mat. Res. Soc. Symp. Proc.* 46, 111 (1985)
7. L.V.C. Assali and J.R. Leite, *Phys. Rev. B* 36, 1296 (1987)
8. G.W. Ludwig and H.H. Woodbury, *Phys. Rev. Lett.* 5, 98 (1960)
9. H.H. Woodbury and G.W. Ludwig, *Phys. Rev.* 117, 102 (1960)
10. G.W. Ludwig and H.H. Woodbury, *Solid State Physics* 13, 223 (1962)
11. J.J. van Kooten, G.A. Weller and C.A.J. Ammerlaan, *Phys. Rev. B* 30, 4564 (1984)
12. W. Gehlhoff and K.H. Segsa, *Phys. Stat. Sol. (b)* 115, 443 (1983)
13. W. Gehlhoff, K. Irmscher and J. Kreissl, *this volume*
14. J.W. Corbett, private communication
15. T.M. Dunn, *Transactions Faraday Soc.* 57, 1441 (1961)
16. F.S. Ham, *Phys. Rev.* 138, A1727 (1965)
17. F.G. Anderson, Ph.D.-thesis, Lehigh University, 1987
18. A. Abragam and M.H.L. Pryce, *Proc. Roy. Soc. (London)* A206, 173 (1951)
19. C.E. Moore, *Atomic Energy Levels*, Natl. Bur. Stand. (U.S.) *Circ. No. 467*
20. J.J. van Kooten, E.G. Sieverts and C.A.J. Ammerlaan, to be published
21. G.D. Watkins, *Phys. Rev.* 155, 802 (1967)
22. J.R. Morton and K.F. Preston, *J. Magn. Resonance* 30, 577 (1978)
23. G.W. Ludwig and H.H. Woodbury, *Phys. Rev.* 117, 1286 (1960)
24. R.E. Watson and A.J. Freeman, in *Hyperfine Interactions*, edited by A.J. Freeman and R.B. Frankel (Academic, New York, 1967), p. 53